10. S. Hild et al., "Sensitivity studies for third-generation gravitational wave observatories," Class. Quant. Grav. **28**, 094013 (2011).
11. A. Khalaidovski, "Beyond the quantum limit: a squeezed-light laser in GEO 600," Ph.D. thesis, Leibniz University Hannover (2011).
12. H. Vahlbruch, S. Chelkowski, B. Hage, A. Franzen, K. Danzmann, and R. Schnabel, "Coherent control of vacuum squeezing in the gravitational-wave detection band," Phys. Rev. Lett. **97**, 011101 (2006).
13. K. McKenzie, E. E. Mikhailov, K. Goda, P. K. Lam, N. Grosse, M. B. Gray, N. Mavalvala, and D. E. McClelland, "Quantum noise locking," J. Opt. B: Quantum S. O. **7**, S421–S428 (2005).
14. H. Grote and the LIGO Scientific Collaboration, "The GEO 600 status," Class. Quant. Grav. **27**, 084003 (2010).
15. S. Hild, H. Grote, J. Degallaix, S. Chelkowski, K. Danzmann, A. Freise, M. Hewitson, J. Hough, H. Lück, M. Prijatelj, K. A. Strain, J. R. Smith, and B. Willke, "DC-readout of a signal-recycled gravitational wave detector," Class. Quant. Grav. **26**, 055012 (2009).
16. H. Vahlbruch, A. Khalaidovski, N. Lastzka, C. Gräf, K. Danzmann, and R. Schnabel, "The GEO 600 squeezed light source," Class. Quant. Grav. **27**, 084027 (2010).
17. M. Mehmet, H. Vahlbruch, N. Lastzka, K. Danzmann, and R. Schnabel, "Observation of squeezed states with strong photon-number oscillations," Phys. Rev. A **81**, 013814 (2010).
18. E. Oelker, L. Barsotti, S. Dwyer, D. Sigg, and N. Mavalvala, "Squeezed light for advanced gravitational-wave detectors and beyond," Opt. Express **22**(17), 21106–21121 (2014).
19. H. Wittel, H. Lück, C. Affeldt, K. L. Dooley, H. Grote, J. R. Leong, M. Prijatelj, E. Schreiber, J. Slutsky, K. Strain, M. Was, B. Willke, and K. Danzmann, "Thermal correction of astigmatism in the gravitational wave observatory GEO 600," Class. Quant. Grav. **31**, 065008 (2014).
20. E. Schreiber, K. L. Dooley, H. Vahlbruch, and H. Grote, "Alignment sensing and control of squeezed states of light," in preparation.

1. Introduction

The dominant broadband noise source for the advanced laser interferometric gravitational wave (GW) detectors will be quantum noise [1–3]. The classical method for reducing quantum noise at shot-noise-limited frequencies is to increase the laser power. Higher laser power, however, introduces many technical challenges arising from laser light absorption and subsequent heating of the optics. Another approach to reduce quantum noise is to inject squeezed states of light into the interferometer's anti-symmetric port, a technique which reduces the measurement uncertainty in the readout signal [4]. Rapid advances in both squeezing technology and laser interferometer development in the last decade resulted in the first demonstrations of this quantum noise reduction technique on current interferometric GW detectors in 2010 at GEO 600 [5] and in 2011 at LIGO Hanford [6].

GEO 600 is carrying out the first long-term study of incorporating squeezed states of light in a GW detector. Results include demonstration of a squeezing duty cycle of 90% with mean detected squeezing of 2.0 dB during an 11 month data collection period in 2012 [7]. Continued work since then has resulted in an increase of the observed squeezing level up to a maximum of 3.7 dB to date and a continued high duty cycle of 85% [8]. This study has demonstrated the readiness of squeezed states of light as a permanent application for increasing the astrophysical reach of GW detectors. Projects such as Advanced LIGO and Advanced Virgo are now making plans to incorporate squeezing as an early instrumental upgrade.

The limits to the level of non-classical noise reduction that can be achieved depend on the following four variables: degree of generated squeezing, optical losses (including beam alignment and mode-matching), phase noise, and noises in the squeezing frequency band other than shot noise. This paper focuses on new techniques developed, implemented, and analyzed at GEO 600 which serve to reduce phase noise.

Phase noise refers to any root-mean-square (rms) difference between the angle of the squeezing ellipse and the angle of the measurement quadrature of the interferometer as depicted in Fig. 1. The degree of measurable squeezing and anti-squeezing is reduced for an rms phase noise of $\phi \ll \pi$ as follows:

$$V_s' = \quad V_s \cos^2 \phi + V_a \sin^2 \phi \tag{1}$$

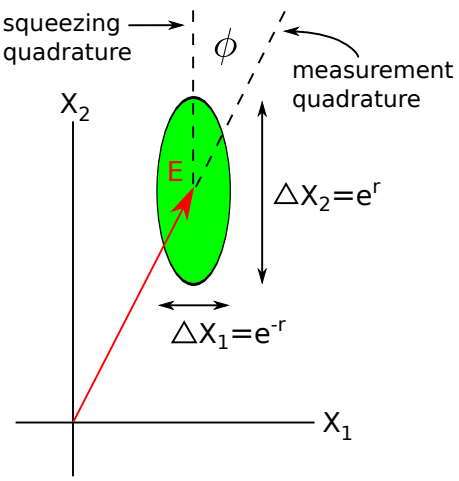

Fig. 1. Phasor diagram of a squeezed state ($\Delta X_1 \Delta X_2 \geq 1$). The factor r describes the degree of squeezing and anti-squeezing for a pure state and ϕ describes the mismatch in angle between the squeezing and measurement quadratures. For application in a GW detector, phase squeezing is injected to the anti-symmetric port.

$$V_a' = \quad V_a \cos^2\phi + V_s \sin^2\phi \tag{2}$$

where V_s and V_a are the variances of the squeezed and anti-squeezed states, respectively, before including the effect of phase noise.

Phase noise, also called 'quadrature fluctuations' or 'squeezing angle jitter', is one of the limits to quantum noise reduction that already affects today's squeezing enhanced interferometers. During regular squeezing operation at GEO 600, there are approximately 37 mrad rms phase noise. With optical losses of about 40%, this phase noise reduces the observed squeezing level by a few tenths of a dB compared to no phase noise at all. In the extreme case, too much phase noise can even result in anti-squeezing, as was observed during the squeezing experiment at LIGO Hanford when a high non-linear gain was intentionally used [9].

As optical losses are lowered, phase noise becomes more critical. Anti-squeezing grows larger and its projection onto the squeezed state thus also grows larger for a given angle. To achieve 6 dB of squeezing as is intended for advanced detectors, phase noise must be no more than 10 mrad rms if optical losses are 25%. However, with a push to only slightly lower optical losses, such as 20%, as much as 30 mrad phase noise can be tolerated. Third generation detectors, which have goals of 10 dB of squeezing [10], will require that phase noise be at most only a couple mrad rms. Here, a critical boundary is that losses of 10% would already require there be no phase noise at all.

Both static mismatch and relative motion at all frequencies between the squeezing and measurement quadratures contribute to the rms phase noise. Temperature-induced path length fluctuations, swinging suspended optics, and phase modulation from radio frequency (RF) sidebands account for some of the sources of phase noise. Calculations of these and other effects are presented in Ref. [9]. Described in the context of a phase noise sensing and control system, the total phase noise can be grouped into contributions from four frequency bands:

- DC: lock point errors
- in-loop frequencies: integrated rms within the control band

#226813 - $15.00 USD Received 21 Jan 2015; revised 6 Mar 2015; accepted 9 Mar 2015; published 23 Mar 2015

- audio frequencies: phase noise outside of the control band
- radio frequencies: RF sidebands used for interferometer control create phase noise on the GW carrier

Efforts to minimize phase noise at GEO 600 are three-fold. First, steps are taken to build an intrinsically quiet squeezing source to limit the amount of fluctuations of the squeezing ellipse at its generation. This includes considerations in the mechanical design of the optical parametric amplifier (OPA) as well as the implementation of a pump phase control loop for stabilizing the squeezing angle when it is created. Overall, the GEO 600 OPA produces a squeezing ellipse with 9 mrad rms phase noise [11]. Second, this stable squeezed field is in turn stabilized with respect to the GW carrier at the interferometer output port using coherent control sidebands (CCSBs) on the squeezed field [12]. Third, drift of the squeezing angle which cannot be sensed properly by the coherent control loop is counteracted at frequencies < 10 mHz through a noise locking technique [13] to maximise the strain sensitivity. The combination of the noise lock with coherent control is new, and was pivotal for long-term squeezing [7].

Historically, both at GEO 600 and at LIGO Hanford, the phase error signal was derived from the beat between the squeezer CCSBs and the interferometer carrier light at a 1 % pick-off mirror before the output mode cleaning cavity (OMC) [5, 6]. This signal has both susceptibility to lock point errors due to higher order modes (HOMs) and has a limited signal to noise ratio (SNR). We present our study and experimental demonstration at GEO 600 of the advantages of two alternative techniques of generating coherent control phase error signals.

This paper is organized as follows: Section 2 provides an overview of the experimental setup; Section 3 introduces the three phase error signals and discusses their respective merits and drawbacks; Section 4 presents our experimental results; and Section 5 discusses implications for the design of future squeezing-enhanced GW detectors. The paper finishes with a summary in Section 6.

2. Experimental setup

Figure 2 shows a schematic of the GEO 600 interferometer together with the squeezing source and highlights how the three different phase error signals are generated. The optical layout of GEO 600 is depicted in the upper left corner. GEO 600 is a power- and signal-recycled Michelson interferometer with folded arms within 600 m long beam tubes [14]. Gravitational waves phase modulate the carrier light in the Michelson arms and the resulting audio frequency sidebands are coupled out to the anti-symmetric port of the interferometer. The Michelson is operated with a small dark fringe offset so that some carrier light leaks to the anti-symmetric port and serves as a local oscillator for the GW sidebands [15]. Beam directing and mode-matching optics send this light to the OMC to filter out HOMs and RF control sidebands. The GW signal is encoded as power variations of the light transmitted through the OMC and is detected by an in-vacuum photodetector (PD).

The GEO 600 squeezed light source is installed on an in-air table next to the vacuum tank containing the OMC and readout PD. A series of steering mirrors directs the squeezed field to the open port of the polarizing beam splitter (PBS) of the in-vacuum Faraday isolator (FI) in the interferometer output chain. Located directly in front of the OMC, the PBS directs the squeezed field backwards through the FI, rotating its polarization to match that of the interferometer carrier. The squeezed vacuum is then reflected off of the over-coupled signal recycling cavity (SRC) and joins the GW local oscillator field on the detection PD.

For the generation and control of squeezed vacuum states, three phase-locked lasers are used (only two of which are indicated in Fig. 2). A fraction of the main squeezer laser at 1064 nm is frequency doubled in a second-harmonic generator (SHG) which provides the required pump

#226813 - $15.00 USD Received 21 Jan 2015; revised 6 Mar 2015; accepted 9 Mar 2015; published 23 Mar 2015

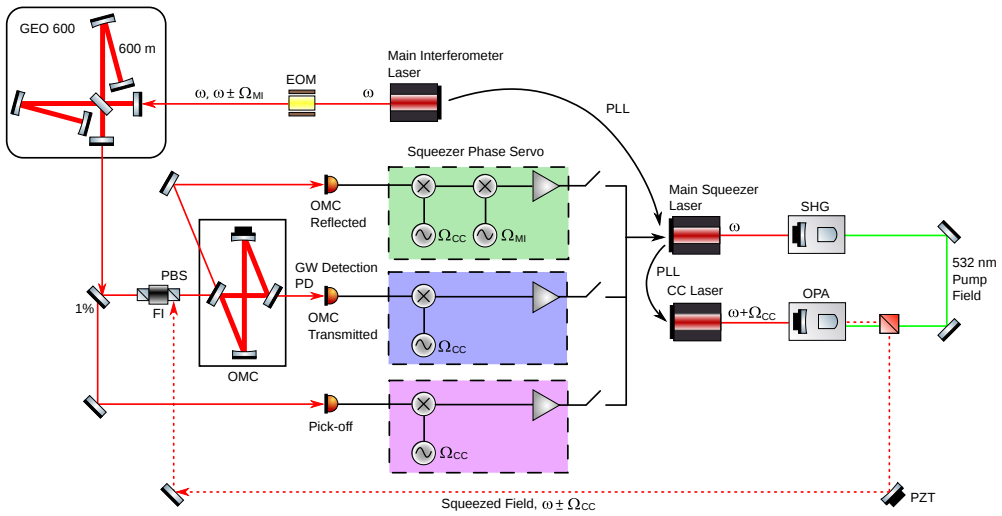

Fig. 2. Schematic of the GEO 600 interferometer together with the squeezing source. The three methods presented in this article for generating a squeezer phase error signal are highlighted: OMC reflected, OMC transmitted, and pick-off. Only one path is used at a time and the control signal is fed back to the error point of the PLL which locks the main squeezer laser to the interferometer main laser. Complete phase control is accomplished through the following two additional stages: locking of the green pump beam phase to the OPA and a noiselock loop.

field at 532 nm for the non-linear squeezing resonator. One of the control lasers (not shown) locks the OPA length. The other control laser (labeled 'CC') is injected into the locked OPA to stabilize the angle of the squeezing ellipse with a bandwidth of 7 kHz. This process generates the CCSBs which have a stable phase with respect to the correlated audio sidebands [12]. The CCSBs thus serve as a marker of the squeezing angle and co-propagate with the squeezed field. The CCSB frequency, $f_{\mathrm{CC}} = 15.2$ MHz, is chosen so as to be anti-resonant in the GEO SRC. A detailed description of the GEO 600 squeezer is found in Ref. [16].

The three methods for generating a squeezer phase error signal are featured in the center of Fig. 2 and will be discussed in detail in the next sections. The error signal is fed back to change the frequency of the squeezer main laser, which acts as a phase actuator with a $1/f$ response. A gain is selected to give a bandwidth of about 2 kHz and some filters are included to provide additional suppression below 30 Hz.

3. Phase error signal

The squeezer phase error signal is contained in the beat between the TEM_{00} modes of fields which carry phase information about the GW carrier and the squeezed vacuum, respectively. Potential signals are derived not only from various choices of reference fields, but also from a selection of ports where these fields are available. We evaluate the following three methods of generating a squeezer phase error signal with respect to the GW measurement quadrature:

- CCSBs vs. carrier at pick-off port
- CCSBs vs. Michelson sidebands in OMC reflected
- CCSBs vs. carrier in OMC transmitted

#226813 - $15.00 USD Received 21 Jan 2015; revised 6 Mar 2015; accepted 9 Mar 2015; published 23 Mar 2015

We refer to the signals as 'pick-off', 'OMC reflected', and 'OMC transmitted', respectively, where the latter two are the new alternative techniques.

The squeezer CCSBs are used as a reference of the squeezer phase in all scenarios because the squeezed field itself cannot be used to generate an error signal. It contains only several photons per second [17] and such a low amplitude field cannot be measured directly on a photodetector. In addition, the interferometer output field contains not only the local oscillator for the GW signal, but also the interferometer RF control sidebands which serve as a phase reference of the carrier light. Both the carrier and the Michelson (MI) sidebands are thus candidates for representing the squeezing quadrature to generate a phase signal. One feature of GEO 600's MI sidebands ($f_{\mathrm{MI}} = 14.9$ MHz) is that they are spatially cleaner than the carrier field at the output port. This is due to the Schnupp asymmetry, which gives the MI sidebands a much larger dark fringe offset than that for the carrier light. As a result, the TEM_{00} mode of the MI sidebands dominates over the higher order mode content of the MI sidebands. Whether the MI sidebands are spatially cleaner than the carrier in other interferometers depends on the individual optical layout and the quality of the optics.

If present, higher order modes play a central role in the quality of the error signals both through increasing the shot noise but not the signal and through creating an offset to the lock point of the loop. We define *lock point errors* as non-intentional contamination of the proper phase signal with false information which pushes the system away from the nominal operating point. Because these offsets originate on the sensor and are thus in-loop, they cannot be suppressed by the loop. Intrinsic HOM content of either the local oscillator or reference fields, mode-mismatch of the fields, and beam misalignment are all relevant factors for creating lock point errors. Detailed calculations and additional discussion are presented in Ref. [18].

The SNR for a given phase error signal is defined as:

$$\mathrm{SNR} \propto \frac{E_1 E_2}{\sqrt{P}} \tag{3}$$

where E_1 and E_2 are the amplitudes of the signal fields and P is the total power on the PD, which is valid as long as the sensor is shot-noise-limited. A high SNR allows in-band phase noise to be reduced: for a given bandwidth of a sensor-noise-limited servo, there is a linear relationship between noise floor reduction and in-band rms noise reduction. The most pertinent factors to consider for achieving high SNR are the existence of HOMs and port selection. HOMs contribute to the total power (i.e. noise) but not to the signal and can be reduced through the use of mode cleaning cavities. Additionally, improvements in SNR can come from selecting ports that have a favorable transmission of the signal fields.

Table 1. Schemes studied for generating a squeezer phase error signal. Signal-to-noise ratios are compared as well as the likelihood of lock point errors as determined by the quantity of HOMs in the signal fields. Field amplitudes and the SNR are normalized to 1.

	Pick-off (1%)	OMC refl.	OMC trans.
fields	[CCSB, carrier]	[CCSB, MISB]	[CCSB, carrier]
amplitudes	[0.1, 0.1]	[1.0, 0.3]	[0.1, 1.0]
frequency	15.2 MHz	300 kHz	15.2 MHz
total power	0.4 mW	30 mW	6 mW
SNR	1/4	1	2/3
HOMs	84%	$< 1\%$	$\ll 1\%$

The pick-off before the OMC is a 1% power transmissive mirror which is nominally in place to extract alignment signals for the MI interferometer. All of the light experiences this 1%

#226813 - $15.00 USD Received 21 Jan 2015; revised 6 Mar 2015; accepted 9 Mar 2015; published 23 Mar 2015

transmission. The OMC rejects a significant fraction of the CCSBs and MI sidebands in addition to HOMs. Thus, all fields except the carrier TEM_{00} are in the OMC reflected port. The carrier is entirely transmitted. The OMC finesse of 150 is sufficiently low, however, such that the CCSBs and MI sidebands do have a power transmission of 1%. The CCSBs are thus available at all three ports, although to varying extents, which plays a role in the available SNR. Furthermore, although the MI sidebands have intrinsically less HOM content than the carrier, the carrier is stripped of its HOMs by the OMC, making it a promising signal at this transmission port.

Based on the pick-off fractions at each port and measurements of the power in the GEO 600 output beam [19], the SNRs of the three signals are computed and displayed in Table 1. Of the approximately 37 mW in the GEO 600 output port beam, about 6 mW are carrier light in the TEM_{00} mode and approximately 0.6 mW are Michelson sidebands. The remainder are HOMs, predominantly at the carrier frequency. The highest of the field amplitudes and SNRs are normalized to 1 to allow easier comparison of signals. The fraction of the total power in each reference field that is made of HOMs is also presented. For the pick-off signal, this is based on power measurements. For the OMC reflected signal, where HOMs of only the Michelson sideband light are of interest, OMC mode scans using two different sideband powers provides the upper limit of 1%. The percentage of carrier HOMs in the OMC transmitted light is computed based on the OMC g-factor and finesse and the mode content of the output port beam.

In terms of both SNR and susceptibility to lock point errors, we find that the pick-off signal is the worst option. For GEO 600 the signal in OMC reflected has a 4-fold higher SNR and less HOM content. The signal in OMC transmission has more than a factor two higher SNR and almost no HOM content. The reduction of HOMs in the signal is a very important feature in that it holds the promise of eliminating lock point errors, a critical problem that was encountered in the LIGO squeezing demonstration [9] and to a lesser extent at GEO 600 due to the addition of a squeezer alignment system [20].

4. Experimental results

We experimentally demonstrate the reduced lock point errors of the two new phase error signals using the squeezing-enhanced GEO 600 detector. We built and installed the appropriate electronics and photodiodes as depicted in Fig. 2 and commissioned each of the control loops. As the signals cannot be used simultaneously, results were obtained by switching consecutively from one signal to the next on a seismically quiet evening during a single lock stretch to ensure the fairest possible comparisons. Twenty-minute long data stretches were acquired for each signal and the reproducibility of the results were verified by repeating the entire experiment on several occasions. The auto-alignment system for the squeezer was used and the squeezer tuned to achieve about 3.2 dB, the highest squeezing level possible at the time.

Figure 3 shows a representative example of the free running, in-loop, and sensing noise spectra of the squeezer phase error signal. The free-running spectrum was computed based on the measured in-loop spectrum and a model of the open loop transfer function. The sensing noise spectrum is taken when a shutter in the optical path of the squeezed field is closed and thus no squeezing applied. All spectra are calibrated to $\mathrm{rad}/\sqrt{\mathrm{Hz}}$ using the measured peak-to-peak amplitude V_{pp} of the free-running error signal. The calibration factor is $1/(V_{pp}/2)$. In addition, a calibration line is injected at 6500 Hz by actuating on the squeezing phase via a PZT mounted on a steering mirror in the squeezer path. This line serves as a calibration monitor of the running system and its amplitude is selected so that its contribution to rms phase noise is insignificant.

This particular example is from the OMC transmission signal. Equivalent spectra from the pick-off and OMC reflection signals are nearly identical and feature only different sensing noise

#226813 - $15.00 USD Received 21 Jan 2015; revised 6 Mar 2015; accepted 9 Mar 2015; published 23 Mar 2015

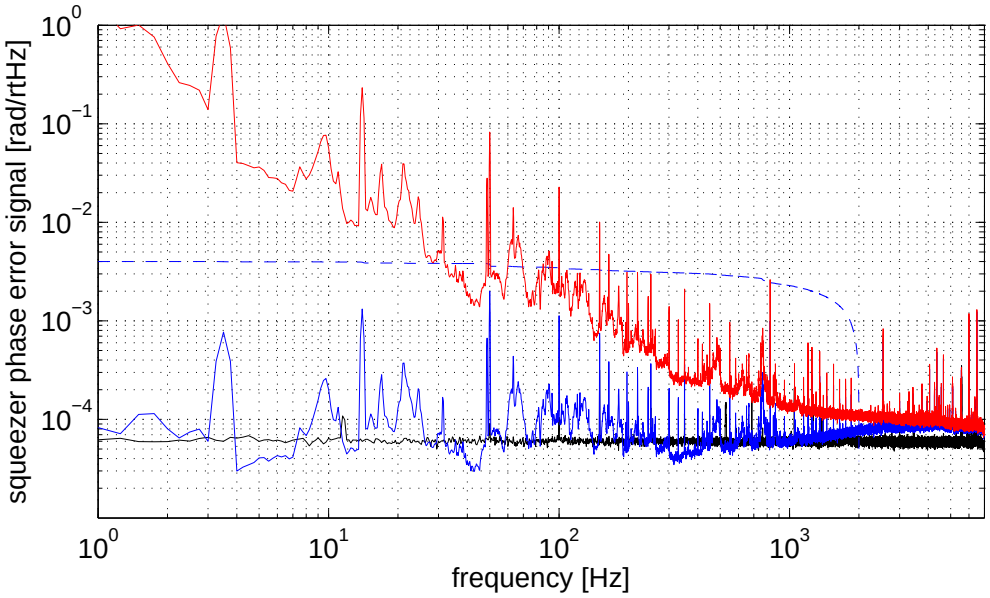

Fig. 3. Phase noise detected by the beat of the CCSBs and the carrier light in OMC transmission. The in-loop error signal (blue) is suppressed to or below sensor noise (black). The free-running phase noise (red) is computed from the in-loop spectrum and the known loop shape. The dashed line shows the integrated rms within the control band of 2 kHz. The in-loop phase noise is 4 mrad rms. Spectra are created from a digitally-acquired 240 sec long time series with 0.25 Hz binwidth and 120 averages.

floor levels. Unfortunately, the experimental setup does not fully reflect the ideal scenario for which SNRs were calculated in Table 1 such that a direct comparison of noise floor levels to predicted SNR cannot be made. For instance, none of the sensors are shot-noise-limited; electronics noise sits close below sensor noise in all scenarios. In the case of OMC transmission, this extra noise has been tracked to RF pick-up problems with the photodiode setup. Furthermore, in generating the signal in OMC reflection, only some fraction of the available light is used.

The magnitude of the effect of extra electronics noise on the total in-loop phase noise is of interest. A measurement of dark noise indicates that the shot-noise-limit is 25% below sensor noise. The in-loop phase noise contribution is computed from the quadrature sum of the error signal and sensor noise starting at the loop's unity gain frequency of 2 kHz. It is 4 mrad rms, but could be reduced to 3 mrad rms should the RF pick-up noise in this setup be reduced.

Figure 4 highlights the main result of this paper, which is that the OMC transmission and OMC reflection phase error signals eliminate lock point errors and create a squeezing level which is stationary in time. The band-limited rms (BLRMS) spectra for a shot-noise-limited region between 4 kHz and 5 kHz of the GEO 600 strain sensitivity is plotted for a non-squeezed time as well as squeezed times when each of the various phase error signals were used. If the total rms phase noise changes in time, then there will be fluctuations of the squeezing level and therefore of the shot-noise-limited strain sensitivity. There are both linear and quadratic couplings of the squeezing angle fluctuations to the frequencies in this spectrum, depending on the frequency content and amplitude of the fluctuations.

Notably, the spectrum of the shot noise BLRMS when the OMC transmission and OMC

#226813 - $15.00 USD Received 21 Jan 2015; revised 6 Mar 2015; accepted 9 Mar 2015; published 23 Mar 2015

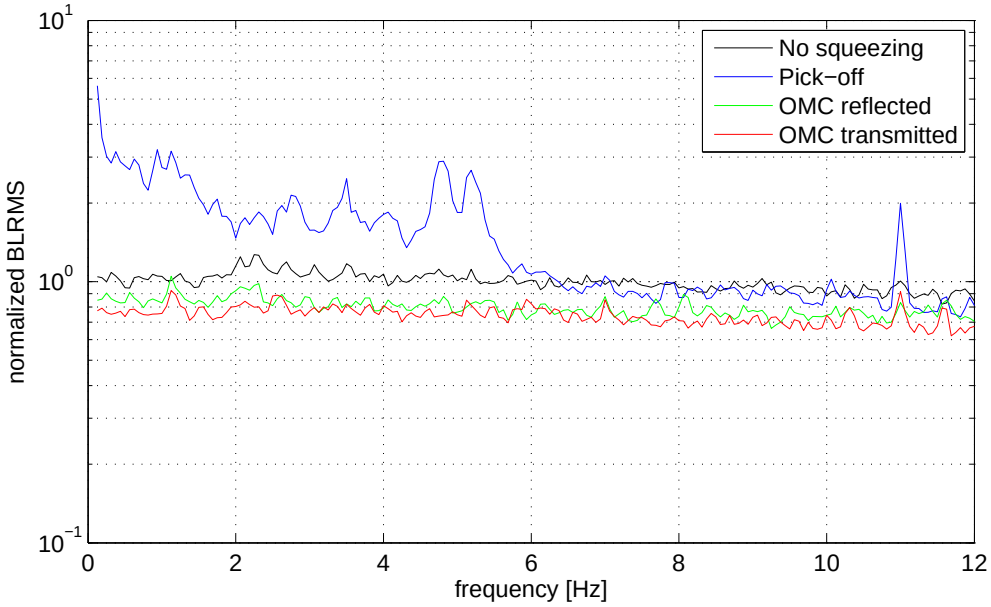

Fig. 4. Amplitude spectra of the band-limited-rms of strain sensitivity in a shot-noise-limited frequency band from 4 kHz to 5 kHz. Stability of the squeezing level when using the OMC transmission and OMC reflection signals is demonstrated. The increase in fluctuations of the squeezing level when the standard pick-off signal is used is due to lock point errors from HOMs. All spectra are normalized to the mean of the non-squeezed spectra and the relative levels indicate the amount of squeezing present. Note, however, that the squeezing level is not always perfectly steady in time, so the levels in this figure do not necessarily represent the best possible squeezing.

reflection signals are used is no different than that from the non-squeezed time. Only the DC level differs, which is the desired effect of squeezing. Furthermore, this demonstrates that the total rms phase noise from in-band and RF frequencies is very stable on these time scales. The effect of lock point errors from the pick-off signal is largely observed at frequencies below 6 Hz where the suspended output optics are swinging and altering the spatial distribution of HOMs on the sensor. These high levels of phase noise are not so frequent, so the effect on the average squeezing level is small. Nonetheless, stationarity of the data is of great importance for gravitational wave searches.

Table 2. Phase noises from known sources when the OMC transmitted signal is used. The quadrature sum is 16.1 mrad rms.

source	rms phase [mrad]
in-loop: up to 2 kHz	4
audio: 2 kHz – 45 kHz	13
RF: 14.9 MHz MI sidebands	6.7
RF: 9 MHz SRC sidebands	5.5

Finally, Table 2 presents a break down of the known phase noise contributions from different frequency bands. The audio band phase noise comes from computing the square difference between the signal and the sensor noise in the OMC transmitted signal from a measurement out

#226813 - $15.00 USD Received 21 Jan 2015; revised 6 Mar 2015; accepted 9 Mar 2015; published 23 Mar 2015

to 45 kHz. Above 45 kHz, the signal is sensor-noise-limited. Phase noise from the 1% of RF sidebands that get transmitted through the OMC is computed [9] based on a measurement of the power in the sidebands and the 5% ratio of contrast defect to dark fringe offset. Upon adding these contributions incoherently, we find that we have a total known phase noise of 16.1 mrad rms. Phase noises which cannot be measured directly such as phase noise in the frequency band above 45 kHz and lock point errors are not included. An out-of-loop measurement of phase noise when using the OMC transmitted signal indicates the total phase noise is 37 ± 12 mrad rms.

5. Discussion

Table 3 shows a summary of the various experimental parameters that play a role in determining the quality of each of the phase error signals. The most important new implications that this work generates for interferometer design are related to the OMC and PD readout electronics. The OMC finesse and the CCSB frequency can be selected to allow a greater fraction of the CCSBs to be transmitted through the OMC than the current 1% transmission at GEO 600. A trade-off must be reached, however, between lowering the OMC finesse to let more CCSBs through and preserving its function as a filter for both HOMs and the interferometer RF sidebands. There are also technical limitations to how low of a frequency the CCSBs can be. Because the CCSBs have the same polarization as the squeezed field, power noise on the CC field that extends into the GW frequency band can reduce the squeezing generated at the OPA by seeding on top of the vacuum seed. Some of this power noise could be alleviated by stabilizing the CC laser.

Table 3. Important aspects to take into consideration when selecting which of the three squeezing angle error signals to use and when thinking about how to improve them.

	Pick-off	OMC refl.	OMC trans.
HOMs (carrier)	×		
HOMs (MI SBs)		×	
HOMs (alignmnent)	×	×	
CCSB frequency			×
CCSB amplitude	×	×	×
MI SB amplitude		×	
Pick-off fraction	×		
OMC finesse			×

Another aspect of using the OMC transmitted phase signal is that the information is carried on the same light that carries the GW signal. To maintain the highest possible detection efficiency, the two signals must be detected using the exact same PD(s). While DC readout of the GW signal requires only low-noise DC electronics, low-noise RF electronics are needed in addition in order to recover the squeezer phase error signal. This introduces the challenge of having to design and build dual low noise DC and RF readout electronics that are also not susceptible to RF pick-up. This represents current on-going work at GEO 600.

Although the OMC reflected phase signal is a good option for GEO 600, it is not necessarily the case for other detectors. The amount of MI sideband HOMs will need to be evaluated for each individual experimental setup. Also, the MI sidebands do intrinsically contribute to phase noise at RF frequencies and a trade-off in the level of MI sidebands is required. In addition, it should be noted that although the SNR argument based on shot noise is irrelevant for GEO 600 at the moment, it could be meaningful in the future and for different detectors.

#226813 - $15.00 USD Received 21 Jan 2015; revised 6 Mar 2015; accepted 9 Mar 2015; published 23 Mar 2015

A nice side effect of eliminating the use of the pre-OMC pick-off for a phase signal is that optical losses can be reduced. Although the pick-off mirror is required for sensing some of the angular degrees of freedom of the interferometer, a lower pick-off fraction can be afforded when the light does not need to be shared with a PD for squeezer phase sensing.

Finally, although we use a noise lock loop to counteract lock point errors, it cannot fully compensate for all of the errors from the pick-off signal due to its limited usable bandwidth of at most 100 mHz. This limitation comes from the implementation of the noise lock, which is to dither the squeezing phase at 11.6 Hz. Higher bandwidth could only come from increasing the dither amplitude, but this itself would add to the rms phase noise. The noise lock loop is thus limited to control unsensed drifts of the squeezing phase only on slow time scales. Upon using the OMC transmitted signal, the noise lock loop corrects for drifts of the squeezing angle on the order of tens of mrad over hour time scales. One underlying cause of these drifts is the fact that the CCSBs are imbalanced. Any change in the relative amplitudes of the CCSBs results in an offset to the locking point. This may arise from changes in non-linear gain which is itself susceptible to influences such as changing laser power.

The phase signals in OMC reflection and OMC transmission have each been used for standard squeezing operation at GEO 600 at different times since 2011. The greater part of the 11 month period reported in Ref. [7] used the OMC reflection signal, and since the last couple of months of that run, the OMC transmitted signal has been in permanent use. After a new signal recycling mirror was installed at GEO 600 which increased the amount of HOMs at the output port and increased lock point errors, the use of these new signals was a critical step for achieving stable squeezing.

6. Conclusion

We proposed two new methods of generating an error signal for matching the longitudinal phase of squeezed states of vacuum to that of the output field of a laser interferometer for gravitational-wave detection. We experimentally compared both of the new methods to the so-far standard method and the new methods are found to be superior. As the main result of this work, we showed that squeezing phase control using either of the new signals eliminates lock point errors and greatly improves the squeezing level stationarity. We discussed other features and advantages of the new methods which contribute to a higher level of observed squeezing and considered some implications for the design of future squeezed-vacuum applications. Having also demonstrated the new methods in long-term application at GEO 600, we conclude that they are a pivotal development towards realizing stable squeezing of 6 dB or more in advanced detectors and beyond.

Acknowledgments

The authors are grateful for support from the Science and Technology Facilities Council (STFC), the University of Glasgow in the UK, the Bundesministerium für Bildung und Forschung (BMBF), and the state of Lower Saxony in Germany. This work was partly supported by the Deutsche Forschungsgemeinschaft, DFG grant SFB/Transregio 7 Gravitational Wave Astronomy. Additionally, we thank Roman Schnabel for leading the effort of providing the squeezer used at GEO 600; Alexander Khalaidovski, Christian Gräf, and Nico Lastzka for their work in building the squeezer and its automation system; Lisa Barsotti and Sheila Dwyer for their respective visits and helpful input; Keita Kawabe for his thoughtful comments on this manuscript; and Michael Weinert, Volker Kringel, Marc Brinkmann and Walter Graß for their work in keeping the GEO 600 interferometer in a good running state for this experiment. This document has been assigned LIGO document number LIGO-P1400150.